 CMES, vol.5, no.1, pp.21-33, 2004

A Micromechanistic Perspective of Cohesive Zone Approach in Modeling Fracture

N. Chandra[1] **and C. Shet**[1]

Abstract: Cohesive Zone Models (CZMs) are increasingly being used to simulate fracture and fragmentation processes in metallic, polymeric, ceramic materials and composites thereof. Instead of an infinitely sharp crack envisaged in linear elastic fracture mechanics, CZM assumes the presence of a fracture process zone where the energy is transferred from external work both in the forward and the wake regions of the propagating crack. In this paper, some of the mechanistic and computational issues in the application of CZM to model failure and fracture in real materials are discussed. In specific we address the issue of CZM in relation to micromechanical processes that are active in and around fracture process zone. We also examine the distribution of total dissipation energy, i.e. inelastic strain energy, and cohesive energy, the latter encompassing the work of fracture and other energy consuming mechanisms within the fracture process zone. It is clearly shown that a thorough understanding of the energetics and underlying micromechanisms of the fracture processes are essential for accurately simulating fracture and failure in materials and structures.

keyword: Cohesive Zone Models, plasticity, finite element method

1 Introduction

In recent years, cohesive zone approaches are finding increasing use in describing fracture and failure behavior in a number of material systems. CZM has been used in the past to study crack tip plasticity, creep under static and fatigue loading conditions, crazing in polymers, adhesively bonded joints, interface cracks in bimaterials, crack bridging due to fibers and ductile particle in composites, among others. CZM was originally proposed by Barenblatt (1959, 1962) as a possible alternative to the concept of fracture mechanics in perfectly brittle materials. Later, Dugdale (1960) extended this concept to perfectly plastic materials by postulating the existence of a process zone at the crack tip.

CZM has spawned a plethora of modeling efforts in the fracture of metals, ceramics, polymers and their composites in the field of engineering mechanics (Needleman, 1990; Rice and Wang, 1989). It is not the purpose of this paper to review all of those models and applications, but outline some of the key works relevant to the present study. Needleman was one of the first to use polynomial and exponential type of traction-separation equations to simulate the particle debonding in metal matrices (Needleman, 1987, 1990). Xu and Needleman (1993, 1994) further used the above model to study void nucleation at the interface of particle and matrix material; fast crack growth in brittle material under dynamic loading; and dynamic crack growth at the interface of bimaterials. Tvergaard (1990) used a quadratic traction-displacement jump form to analyze interfaces. Tvergaard and Hutchinson (1992) used a trapezoidal shape of the traction-separation model to calculate the crack growth resistance. Camacho and Ortiz (1996) employed a linear cohesive-equation fracture model to propagate multiple cracks along arbitrary paths in brittle materials during impact damage. Geubelle et al. (1998) have utilized a bilinear CZM to simulate the spontaneous initiation and propagation of transverse matrix cracks and delamination fronts in thin composite plates subjected to low-velocity impact. In all the CZMs (except Dugdale's model and Camacho et al.'s model) the traction-separation relations for the interfaces are such that with increasing interfacial separation, the traction across the interface reaches a maximum, then decreases and eventually vanishes, permitting a complete decohesion. The main difference lies in the shape and the constants that describe that shape. In this context, the term 'shape' is used in a loose sense to describe the normal (or tangential) traction vs. normal (or tangential) response as typically used in the literature. The magnitude of the parameters in CZMs vary by a factor 10^3 for tractions, energy and for the separation distance. A detailed review of different models in regard

[1] FSU, Tallahassee, FL, USA

with shape, model parameters are discussed elsewhere, see Chandra et al. (2002).

The number of research efforts that use CZM to model fracture process is continuing to increase (Zhang et al. (2002), Allen and Searcy (2001), Eisenmenger (2001), Yang et al. (2001)). There are certain fundamental issues that need to be addressed before CZM can find widespread and unambiguous use to model fracture and fragmentation in materials and structures. They are enumerated below in no particular order of importance.

1. While a generic constitutive equation for the bulk material is written in three dimensions, CZM is expressed in terms of normal/tangential tractions and displacement jumps. This raises certain stress and displacement continuity issues at the interface where the separation occurs.

2. The area under the $T-\delta$ curve in the CZM is generally believed to be the fracture energy. Is this true under all conditions of inelastic deformations within the parent material?

3. It is very clear from our previous work (Tevergaard and Hutchinson, 1992, Li and Chandra, 2003) that the level of plasticity in the bounding material strongly depends on the cohesive strength $\sigma_{\max}$ of CZM. Apart from the local plastic behavior what are the other inelastic characteristics (e.g. damage/cavitation) of the bounding material that affect the fracture response of the material and hence the cohesive zone parameters?

4. Cohesive zone comprises fracture process zone where many different types of inelastic processes occur. These processes are spread over a large region which can be subdivided into forward and wake regions. What is the spatial distribution of energy flow into these regions and how this distribution affect the overall shape of the $T-\delta$ curve?

5. The tail of the $T-\delta$ curve is found to have profound effect on the fracture characteristics of a given material system. It is however, quite different for different failure processes, e.g. particle-matrix decohesion, polymeric, metallic, ceramic matrix composite failures and delamination in thin layered coatings. What is the connection between the micromechanical details of the fracture region and that of the tail of the cohesive zone model?

6. What is the relationship between the shape of the $T-\delta$ curve and the shape of the crack tip. How does the geometry of the tip affect the stress level in the bounding material.

In this paper we seek to address some of the key issues raised here. In section 2 a general interface problem is formulated identifying the constitutive models for the interface and bulk material. In section 3, various micromechanisms that affect the shape of CZM are discussed. An exponential CZM and a geometric model used in the numerical simulation are presented in section 4. Based on the numerical simulation some results are presented in section 5 to answer a few of the specific questions raised above, following which a brief summary is presented in section 6.

2 Formulation of Interface Problem

Consider two solid bodies Ω_1 and Ω_2 separated by a common boundary S as shown in figure 1(a), where S can be considered as the same surface $S_1 \in \Omega_1$ and $S_2 \in \Omega_2$, in the initial configuration, i.e. $S_1 = S_2 = S$. Mathematically, we would like to define S as an infinitesimally thin 3-D domain with surfaces S_1 and S_2 being the part of Ω_1 and Ω_2 before separation occurs. For all practical purposes surface S_1 or S_2 can be identified as a single surface as a part of either of the domains. A material particle initially located (within either of the domain Ω_1 or Ω_2) at some position $\overline{X}$, moves to a new location $\overline{x}$, with a one to one correspondence between $\overline{x}$ and $\overline{X}$ given by the equation of motion $\overline{x} = \chi(\overline{X}, t)$ or $x_i = \chi(X_j, t)$. In a generic sense S defines the interface between the two domains. If Ω_1 is a metal and Ω_2 a ceramic, then S represents a metal-ceramic interface; if Ω_1 and Ω_2 belong to the same material depicting grains of different orientations then S is a grain boundary, and if Ω_1 and Ω_2 represent the same domain $\Omega_1 \cup \Omega_2 = \Omega$, then S is an internal surface which is not yet separated.

In any one of those cases, if S separates to $\acute{S}_1$ and $\acute{S}_2$ (fractures) as shown in figure 1(b), then the process creates new internal/external surface violating the fundamental laws of continuity. Obviously the newly formed region cannot be uniquely mapped from the deformed configuration. The equation of motion of the body $x_i = \chi(X_j, t)$ cannot identify the new region. This is the fundamental problem in modeling fracture (creation of internal/external surface) in the framework of the mechanics

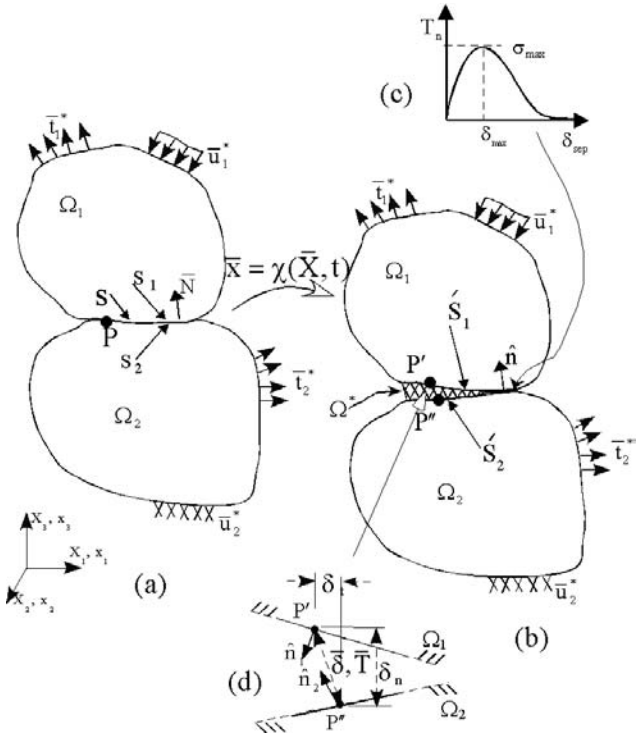

Figure 1 : Conceptual frame work of cohesive zone model.

of continuous medium. The surface S represented by the unit normal $\overline{N}$ ($\overline{N}_1 \in S_1$, $\overline{N}_2 \in S_2$ and $\overline{N} = \overline{N}_1 = \overline{N}_2$) acting along the boundary separating the domain prior to deformation is as shown in figure 1(a). In the deformed configuration as shown in figure 1(d) $\widehat{n}_1$ and $\widehat{n}_2$ represent the unit normal of the surfaces (separated or otherwise). For the domains Ω_1 and Ω_2 the constitutive equation can then be written as

$$\overset{\circ}{\sigma}_{ij} = L_{ijkl}(D_{kl} - D^{In}_{kl}) \tag{1}$$

The elasticity tensor L_{ijkl} is assumed to be isotropic; where D^{El}_{kl}, D^{In}_{kl} are elastic part and inelastic part of rate of deformation tensor ($D_{kl} = D^{El}_{kl} + D^{In}_{kl}$) and $\overset{\circ}{\sigma}_{ij}$ is Jaumann rate of Cauchy stress.

***Interface** S*

If S continues to be a part of Ω_1 and Ω_2 (having points/particles common to both), then the motion of S can be uniquely defined by the motion of either Ω_1 or Ω_2. Though the surface normal $\widehat{N}$ would have rotated and deformed to $\widehat{n}$, in the sense of the kinematics, $\widehat{N} = \Lambda \widetilde{F}^{-1} \widehat{n}$ ($\Lambda = ds/dS =$ stretch ratio, (S, s) is length of a small segment in original and deformed configurations) the motion is unique. Thus we have a one-to-one relationship between the deformed and the undeformed configurations.

If S is to be separated as shown in figure 1(b), then we have created a new surface in the traditional sense of the term. Consider the region bounded by $\acute{S}_1$and $\acute{S}_2$ belonging to a new domain Ω^*. Assume that Ω^* is a 3D domain made of extremely soft glue, which can be shrunk to a surface but can be expanded to a 3D domain. The constitutive relation of Ω^* is expressed quite differently from that of a typical 3-D solid (e.g. Ω_1 or Ω_2). The two surfaces that are initially part of Ω_1 and Ω_2 (S_1 and S_2) have normal $\widehat{N}_1$ and $\widehat{N}_2$ in the undeformed configuration; $\widehat{N}_1$ and $\widehat{N}_2$ are equal and opposite. During deformation the surfaces rotate to new normal $\widehat{n}_1$ and $\widehat{n}_2$. As the surfaces separate we have two surfaces $\acute{S}_1$ ($\acute{S}_1 \in \Omega_1 \cap \Omega^*$) and $\acute{S}_2$ ($\acute{S}_2 \in \Omega_2 \cap \Omega^*$). Constitutive equation is written in term of the normal displacements and tractions. For a narrow region (crack tip region) the directions of $\widehat{n}_1$ and $\widehat{n}_2$ are approximated to be same. A typical constitutive relation of Ω^* is given by $T - \delta$ relations (see figure 1c).

$$\text{if } \overline{\delta} < \overline{\delta}_{sep}, \quad \widetilde{\sigma}\widehat{n} = \overline{T} \tag{2}$$

Beyond a separation distance of $\overline{\delta} > \overline{\delta}_{sep}$, the traction being identically zero within Ω^*,

$$\overline{\delta} \geq \overline{\delta}_{sep}, \quad \widetilde{\sigma}\widehat{n} = \overline{T} = 0 \tag{3}$$

It can also be construed that when $\overline{\delta} > \overline{\delta}_{sep}$ in the domain Ω^*, the stiffness $L_{ijkl} \equiv 0$. In order to implement the vectorial inequalities given in equations 2 and 3, typically separate identities are postulated for the normal and tangential components with limits set for each of them.

The formulation described above can be implemented in a computational scheme like FEM. The advantage of this formulation is that material separation is achieved without loss of continuity. By creating new surfaces, the traction and the stiffness of the cohesive zone elements connecting these newly created surfaces are made to vanish, but the displacements across them are still assumed continuous. On the other hand in computational schemes like node releasing techniques, new surfaces are created using ad-hoc criteria and altering the boundary conditions, which in turn modifies the stiffness arbitrarily.

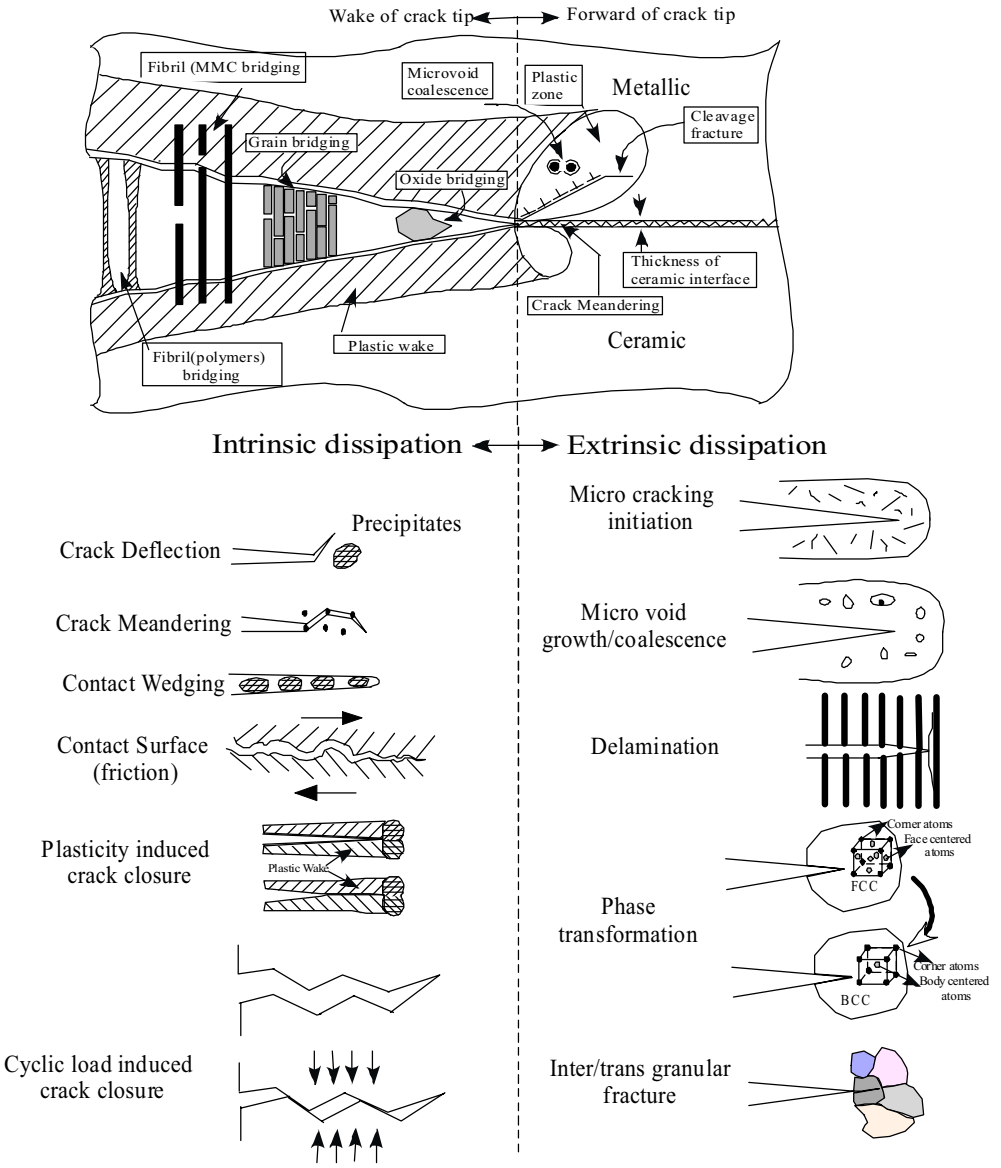

Figure 2 : Energy dissipating micromechanisms in the wake and forward regions.

3 Micromechanics and Shape of CZM

Though various forms of cohesive zone models have been proposed in the past, the qualitative feature shared by all is that as the interface separates for a range of displacements, the magnitude of traction increases, reaches a maximum and beyond that critical length decays until it reaches zero at complete separation. CZM consolidates the effect of a number of intrinsic and extrinsic toughening (or softening) mechanisms occurring within and the immediate neighborhood of the process zone at the tip of a crack. The operative mechanisms depend on the type of material (ductile, brittle, semi-brittle), microstructure (monolithic, composites), temperature and rate of loadings (static, dynamic, cyclic). Ritchie (1999) has suggested that a number of independent (with some dependent) micromechanical processes may be active at the crack tip for ductile and brittle materials, when subjected to either static or dynamic loads. Following this line of thought, figure 2 describes some of the mechanisms that are active in most engineering materials. For the present purpose it can be recognized that intrinsic toughening mechanisms refer to those that occur ahead of the crack tip and extrinsic ones that are behind. We

propose a heuristic argument about why different shapes of cohesive zone models have been proposed in literature and why seemingly some work better than others for a given set of problems.

Let us suppose that a body containing a crack be subjected to external loading. The external work W comprises recoverable elastic energy W_E and irrecoverable dissipative energy W_D

$$W = W_E + W_D \tag{4}$$

Of the dissipative energy, some are used in generating inelastic work in the body Ω_1 and Ω_2 (in terms of plastic work, thermal work) which can be explicitly accounted for, and the rest into the crack tip region. Thus if W_I represents the "accountable" work within Ω_1 and Ω_2 and the rest of inelastic work W_C (within Ω^*), then

$$W_D = W_I + W_C \tag{5}$$

And in this development we are concerned with W_C. W_C represents all the irrecoverable work that flows into crack tip region including the work of adhesion and all other unaccounted work (e.g. heat, sound) that accompanies the deformation. The total work done in the crack tip region W_C can be written as

$$W_C = \Gamma_{ad} + \Psi \tag{6}$$

where Γ_{ad} is the work of adhesion (surface energy) and Ψ is the energy potential describing all the micromechanistic processes active at the crack tip. Let us suppose that there is a total of E extrinsic and I intrinsic processes active and for the sake of simplicity, assume all these processes are dissipative in nature.

Let $\Psi_1, \Psi_2, ...\Psi_E$ and $\Psi_{E+1}, \Psi_{E+2}, ...\Psi_{E+I=N}$ represent the energy potential representing each of the extrinsic $(1, 2, ...E)$ and intrinsic $(E+1, E+2, ...E+I=N)$ processes, then,

$$\begin{aligned} &\Psi = \Psi(\Psi_1, \Psi_2, ...\Psi_N), \quad \text{where} \\ &\Psi_1 = \Psi_1[\delta_1, \Psi_2(\delta), \Psi_3(\delta), ...\Psi_N(\delta)] \\ &\Psi_2 = \Psi_2[\delta_2, \Psi_1(\delta), \Psi_3(\delta), ...\Psi_N(\delta)] \\ &\quad ..... \end{aligned} \tag{7}$$

where it is tacitly assumed that all potentials are evaluated at a given value of δ, measured at an arbitrarily selected but fixed length behind the crack tip. It is also assumed that a given micromechanical response can be determined as a function of its own response and the numerical value of all the processes at that given state. Then,

$$\begin{aligned} \Psi_1(\delta) &= \Psi_1[\delta_1, \Psi_2(\delta), \Psi_3(\delta), ...\Psi_N(\delta)] \\ \Psi_2(\delta) &= \Psi_2[\delta_2, \Psi_1(\delta), \Psi_3(\delta), ...\Psi_N(\delta)] \\ &\quad + ... \end{aligned} \tag{8}$$

where it is presumed that the Ψ_1 can be evaluated at a given value of δ and it is influenced by other micromechanical processes at the identical value of separation displacement. In such cases,

$$\begin{aligned} \frac{\partial \Psi}{\partial \delta} &= \frac{\partial \Psi_1}{\partial \delta} + \frac{\partial \Psi_1}{\partial \Psi_2}\frac{\partial \Psi_2}{\partial \delta} + \frac{\partial \Psi_1}{\partial \Psi_3}\frac{\partial \Psi_3}{\partial \delta} + ... \\ &\quad + \frac{\partial \Psi_2}{\partial \delta} + \frac{\partial \Psi_1}{\partial \Psi_2}\frac{\partial \Psi_2}{\partial \delta} + \frac{\partial \Psi_3}{\partial \Psi_2}\frac{\partial \Psi_2}{\partial \delta} + ... \\ &\quad \frac{\partial \Psi_i}{\partial \delta} + \frac{\partial \Psi_1}{\partial \Psi_i}\frac{\partial \Psi_i}{\partial \delta} + ... \end{aligned} \tag{9}$$

$$\begin{aligned} \frac{\partial \Psi}{\partial \delta} &= \frac{\partial \Psi_1}{\partial \delta} + \frac{\partial \Psi_2}{\partial \delta} + ...\frac{\partial \Psi_i}{\partial \delta} \\ &\quad + \text{cross interaction terms involving } \frac{\partial \Psi_i}{\partial \Psi_j} \end{aligned} \tag{10}$$

Thus the traction at a given δ can be considered as the sum total of tractions at that δ as predicted by the individual micromechanical processes assuming that their cross interaction effects are negligible. For example if $N = 2$ then the total traction due to two interacting micromechanical process can be depicted as shown in figure. 3

If $\Psi = \Psi(t, \delta)$, and $\Psi_1 = \Psi_1(t_1, \delta)$, $\Psi_2 = \Psi_2(t_2, \delta)$....., then the traction $T\rfloor_\delta$ at a given separation distance δ can be written as

$$T\rfloor_\delta = T_1\rfloor_\delta + T_2\rfloor_\delta + ...+ \text{ cross interaction terms.} \tag{11}$$

Since the existence of component of Ψ (e.g. $\Psi_1, \Psi_2....$) depends on individual micromechanism, the shape of the curve depends on the specific problem at hand. Additionally when interaction exists, then terms of the type $\frac{\partial \Psi_i}{\partial \Psi_j}$should also be evaluated.

Experimental evidence There is ample evidence from our own experimental work that some micromechanical aspects of the fracture processes may influence the form of the curve. Thin slice push out test has been extensively

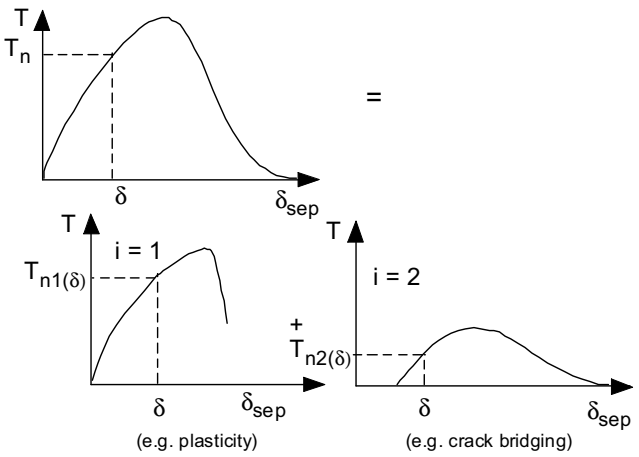

Figure 3 : Total traction T_n is sum of tractions T_{n1} and T_{n2} due to interacting micromechanisims.

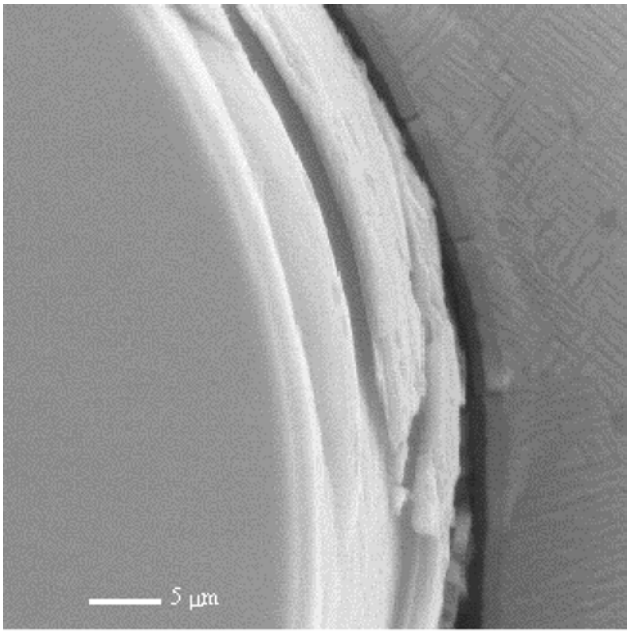

Specimen heat treated at 700^0 C for 25 hours

Figure 4 : Fracture surface formed during push out test on SSC-6/Timetal21s interface.

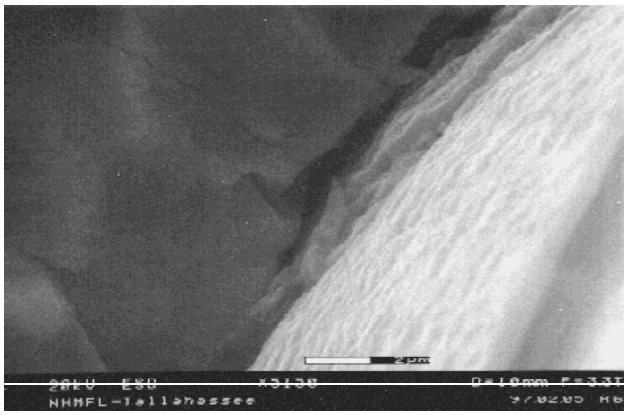

Specimen heat treated at 927^oC for 25 hours

Figure 5 : Fracture surface formed during push out test on SSC-6/Timetal21s interface.

used to characterize the mechanical and fracture properties of ceramic/metal interfaces in metal matrix composites (MMCs). In this test, the composite specimen is sliced to about 500 microns thick with the fibers (about 140 microns diameters) aligned along the thickness direction. A compressive load is applied using a flat indenter to push the fiber out of the specimen. The load is measured as a function of cross head displacement and plotted as $F - \Delta U$ curve. Mukherjee (1997) has conducted the push out tests on MMC, with Timetal21s matrix and SCS-6 fibers (also see Mukherjee et al., 1998). Titanium alloy is highly reactive, and at high temperature reacts with the carbon and silicon in the coating to form reaction zone (interface). Of several test results, two test results are presented here to illustrate the difference in the microstructural features of the interface failure process and corresponding variations in the observed $F - \Delta U$ results.

One sample has been heat treated at 700^oC for 25 hours and the other at 927^oC for 25 hours. Figure 4 shows the fractured surfaces of the matrix fiber interface for 700^oC processed specimen. The fracture surfaces (from several samples processed at 700^oC) reveal that cracks initiate in different regions of the coating, occurring more frequently in the middle and in the region near the coating reaction zone interface. The nature of fracture surface shows a near smooth sharp fracture. Figure 5 shows fractured surfaces of the matrix fiber interface for 927^oC processed specimen. In this case the fracture has taken place along the matrix portion of the interface than in coating. The fracture surfaces are coarse and jagged with presence

of large amount of debris. Figure 6 shows the push out load versus displacement plot for 700^oC processed specimen. It is evident that after reaching a peak load of the order 20 N, there is a sharp load drop (curve drops suddenly), indicating sharp debonding between matrix and fiber and a sharp abrupt fracture process. The acoustic signal confirms that complete debonding occurs at this point. Subsequent rise in curve is due to post fracture frictional sliding between fiber and matrix. The sudden drop in fracture load is because of the reason that the fracture surface is smooth and sharp (Figure 6). Figure 7 shows the push out load-displacement plot corresponding to the 927^oC processed specimen condition. After reaching the peak load the debonding process is slow and gradual. There is no sharp acoustic signal, which marks the complete debonding as recorded in processed specimen. Here the locking of rough surface takes place delaying the debonding process. The fracture process in the processed specimens is characterized by a slow fragmentation of the reaction zone and high peak debond and sliding frictional stresses.

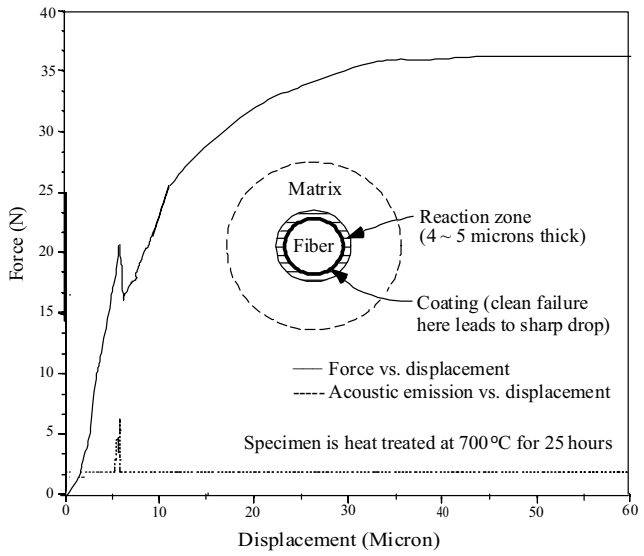

Figure 6 : Typical load displacement curve for a push-out test conducted on $700^o\ C$ processed specimen.

The experimental results show that the failure morphology (surface of failure) changes from smooth (coating) to rough (matrix) leading to two different (sharp vs. gradual) mechanical responses. For a complete discussion of the transition in failure behavior with interface morphology (as a function of heat treatment temperature) the

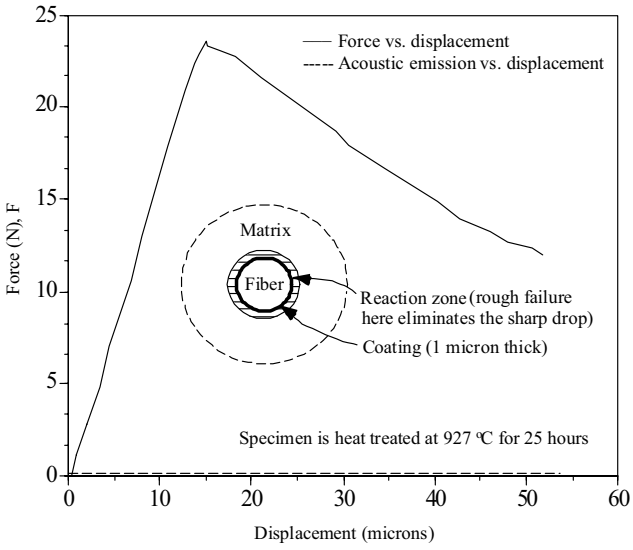

Figure 7 : Typical load displacement curve for a push-out test conducted on 927^oC processed specimen.

reader is referred to Mukherjee et al. (1998). It suffices to point out that interface chemistry and architecture alters the failure response in a thin slice push-out test. Since fracture processes are different, different cohesive zone responses are needed to simulate the behavior. In other words, the observed (or postulated) traction-displacement cohesive response should in some way depend on the micromechanical details at the crack tip. Having said that the various micromechanisims determine the form of the traction-displacement curve, it can be generalized that the shape of CZM is material specific. A CZM with a particular shape that yields good results for one type of material may not do so for other materials. This aspect has been discussed in detail in Chandra et al. (2002) where prediction using bilinear model with specific parameters of metal-ceramic bimaterial interface compares very well with experimental results while exponential model does a very poor job.

4 Selection of CZM and Problem Definition

To study the effect of spatial energy distribution in the fracture process zone, a numerical simulation of fracture in a metallic material is carried out. The interface is characterized by the work of separation and strength in normal and tangential directions. The cohesive zone interface relationship can be expressed such that the tractions

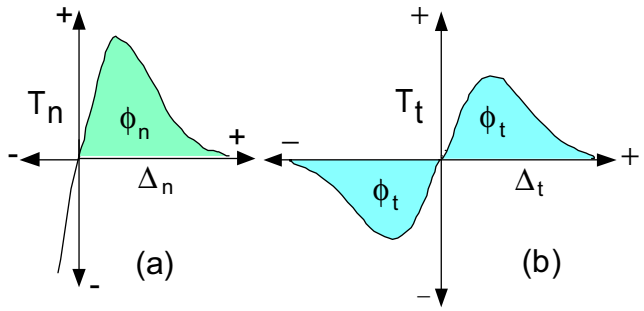

Figure 8 : (a) Variation of nornal traction T_n across the interface as a function of Δ_n when $\Delta_t = 0$, (b) variation of shear traction T_n across the interface as a function of Δ_t when $\Delta_n = 0$.

T across the interface is taken as a function of displacement jump **Δ** across the interface. Defining a work potential of the type $\phi(\Delta_n, \Delta_t)$, such that traction acting in the interface is given by $\mathbf{T} = -\partial\phi/\partial\Delta$. In this work an exponential CZM proposed by Xu and Needleman (1993) is used. The specific potential ϕ is given by,

$$\begin{aligned}\phi(\Delta_n,\Delta_t) = \phi_n + \phi_n \exp(-\Delta_n/\delta_n) \\ \{[1-r+\Delta_n/\delta_n][(1-q)/(r-1)] - \\ [q+[(r-q)/(r-1)]\Delta_n/\delta_n \exp(-\Delta_t^2/\delta_t^2)\}\end{aligned} \tag{12}$$

where $q = \phi_t/\phi_n$, $r = \Delta_n^*/\delta_n$ and ϕ_n = work of normal separation, ϕ_t = work of tangential separation, and Δ_n^* is the value of Δ_n after complete shear separation under the condition of normal tension being zero, $T_n = 0$. The interfacial tractions are obtained as

$$\begin{aligned}T_n = -(\phi_n/\delta_n)\exp(-\Delta_n/\delta_n)\{(\Delta_n/\delta_n) \\ \exp(-\Delta_t^2/\delta_t^2) + [(1-q)/(r-1)] \\ [1-\exp(-\Delta_t^2/\delta_t^2)][r-\Delta_n/\delta_n]\}\end{aligned} \tag{13}$$

$$\begin{aligned}T_t = -(\phi_n/\delta_n)(2\delta_n/\delta_t)(\Delta_t/\delta_t) \\ \{q+[(r-q)/(r-1)]\Delta_n/\delta_n\} \\ \exp(-\Delta_n/\delta_n)\cdot\exp(-\Delta_t^2/\delta_t^2)\end{aligned} \tag{14}$$

The variation of T_n when $\Delta_t = 0$ is as shown in figure 8a; the variation of T_t when $\Delta_n = 0$ is as shown in figure 8 b. The normal work of separation and tangential work of separation are related to the corresponding interfacial strengths $\sigma_{\max}$ and $\tau_{\max}$ respectively and they are given by $\phi_n = \sigma_{\max} e \delta_n$, and $\phi_t = \sqrt{e/2}\tau_{\max}\delta_t$, where $e = \exp(1)$.

The problem of doubled edged notched plate

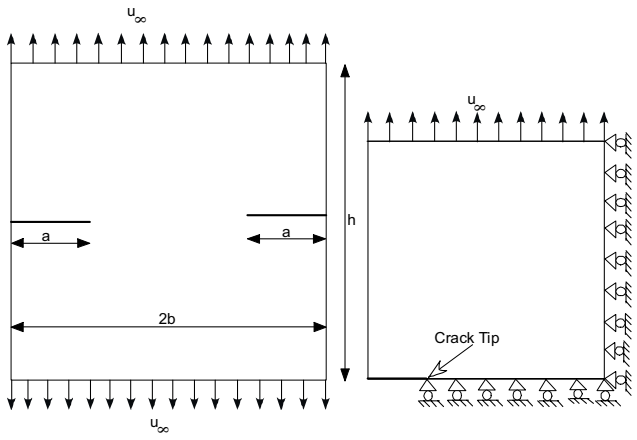

Figure 9 : (a) Double-edge notched plate, (b) geometry and boundary/loading conditions used in FEA model.

For our purpose of computing the energy flow in a fracture process, a double edged notched plate as shown in figure 9(a) is analyzed. Considering the symmetry of loading and geometry, only a quarter portion of the plate as shown in figure 9(b) is discretized. The finite element mesh is as shown in the figure 10(a). The fine mesh around the crack tip is as shown in figure 10(b). The discretized mesh has 24340 plane strain 4 node quadrilateral elements. 7300 cohesive elements with each having 4 nodes are used along the line of crack propagation. A total of 28189 nodes are used to model the geometry. Here the fracture process zone is assumed to be a line, and this line is modeled by 4 node rectangular cohesive elements having zero thickness in the direction normal to the direction of crack propagation. One face of cohesive elements is connected to regular elements while other face is given the symmetric boundary conditions. Thus an artificial interface is created along the line of crack propagation.

The bounding material is assumed to be Al 2024 T3 alloy with the Young's modulus of 72 GPa, Poisson's ratio of 0.33 and the true stress-strain curve is given by $\varepsilon = \frac{\sigma}{E} + \alpha\left(\frac{\sigma}{\sigma_y}\right)^{1/n}$, where σ_y =320 MPa, α =0.01347 and n = 0.217173, fracture toughness K_{IC} = 25 MPa $m^{1/2}$. The cohesive material properties are derived from the global material property of Al 2024 T3. In order to relate the cohesive surface behavior to the fracture toughness, the energy for interfacial normal separation is re-

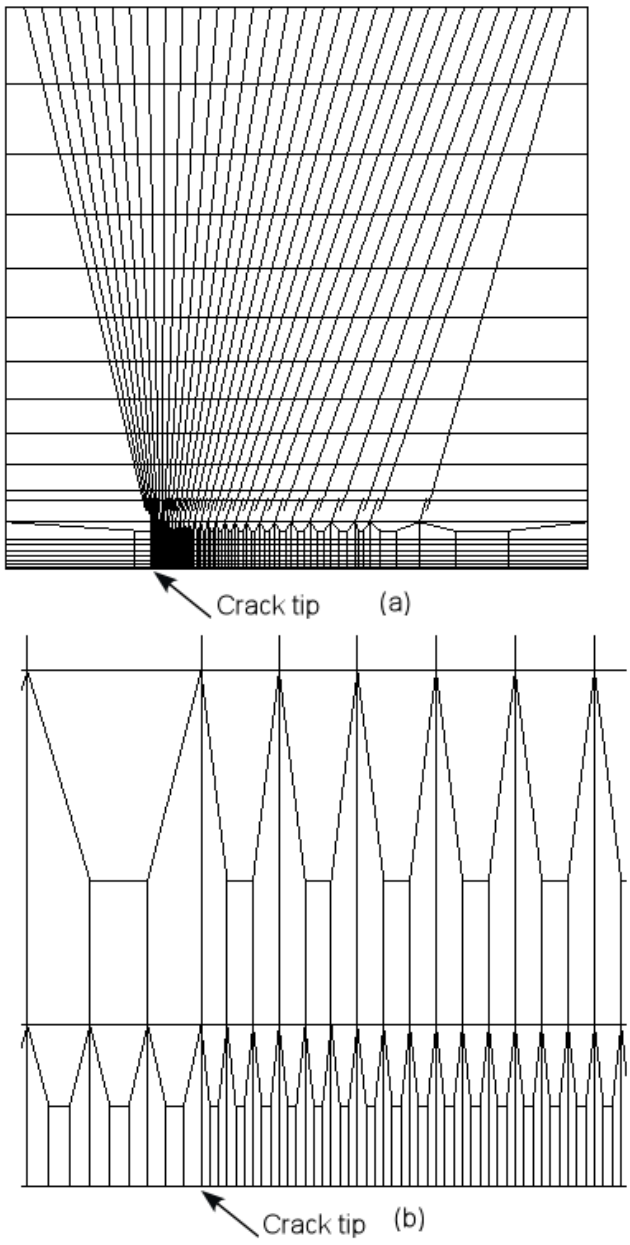

Figure 10 : (a)Finite element mesh model of quarter portion of double edge notched plate, (b) fine mesh near the crack tip.

lated to critical plain strain value of J -integral, $\phi_n = J_{Ic}$ (Rice, (1968)). The maximum cohesive strength is taken as $\sigma_{\max} = \sigma_{ult} = 650.0$ MPa, characteristic normal and tangential displacements $\delta_n = \delta_t = 4.5X10^{-6}$ m, normal and tangential work of separation $\phi_n = \phi_t = 8000$ J. m$^{-2}, r = 0., q = 1$.

Finite Element Simulation

A general purpose finite element code ABAQUS [23] is used for the analysis. Four node elements based on cohesive zone concepts have been developed and implemented as a user defined element within ABAQUS. The crack growth simulation was carried out by applying the far end incremental displacement u_∞. During the application of load the crack tip moves past about 7000 cohesive zone elements. It should be noted that the size of each cohesive zone element is of the order of 5 μm, and corresponds to the characteristic normal displacement δ_n chosen for the problem.

A number of simulations were carried out for a range of cohesive zone properties, especially the cohesive strength. In order to study the effect of cohesive strength on plasticity, $\sigma_{\max}$ was varied such that the ratio of $\sigma_{\max}/\sigma_y$ was varied from 1, 1.5, 2.0 and 2.5. The spatial distribution of energy and plasticity within the bounding material and the cohesive zone were studied to examine the evolution of these quantities as a function of loading history and cohesive strength. All simulations were carried on SGI-Octane with MIPS R12000 Processor running on unix operating system IRIX 6.5, with a typical simulation consuming about 5 to 8 hours of CPU time.

5 Results and Discussion

Energy balance during fracture process

During fracture process the energy is supplied by the external loads. The bounding material undergoes elastic/elasto-plastic deformation involving elastic energy and plastic dissipative energy. If other forms of dissipative processes are modeled within the constitutive equation, then additional energy will be spent in other inelastic processes, for example damage/void growth. In addition to plasticity, energy is supplied to fracture process zone in the form of cohesive energy dissipated within the cohesive elements. This cohesive energy is the sum total of all dissipative processes that go within the crack tip regime, and surface energy. It is understood that traction-displacement curve of cohesive zone model represents only dissipative work and no energy can be recovered during a unloading/reloading condition. For the given system there will be a perfect energy balance between external work and the sum of elastic energy W_E,

plastic dissipative energy W_P and cohesive energy W_C.

$$W_W = W_E + W_P + W_C \tag{15}$$

While W_E and W_P are confined to the binding material, W_C is restricted to fracture process zone (within the cohesive zone elements).

Let us first consider the case of a pure elastic material. The conventional fracture mechanics theory uses the concept of strain energy release rate for crack growth analysis, i.e.,

$$\text{Strain Energy release rate} = G = J = -\frac{\partial U}{\partial a} \tag{16}$$

This fracture energy is dissipative in nature. Hence in an analysis using CZM, even for an elastic material the entire fracture energy of $\phi = J = G = 8000J/m^2$ is dissipated through cohesive elements. In this case, only form of dissipation occurs in cohesive element such that $W_W = W_E + W_C$.

Let us consider the more general case of elasto-plastic materials; two distinct dissipation mechanisms can now be identified, one due to plasticity within the bounding material, and the other due to micro-separation processes in the fracture process zone. There are several micro processes absorbing energy in both the wake and forward regions of the fracture process zone. If the fracture energy $\phi = J = G = 8000J/m^2$ (measured from the experiments for an elasto-plastic material) is to be dissipated, the obvious question that arises is: should the measured fracture energy go entirely into the cohesive zone or should it be split into the two identifiable dissipation processes? It should be realized that during testing when K_{IC} is measured, this value represents the sum total of all dissipative processes in the actual material for initiating and propagating fracture. If the entire fracture energy is used up in the cohesive zone, it will leave no energy for the plastic work in the bounding material. On the other hand, if the fracture energy were to be split into two portions, then in what ratio should that division be made? There seems to be no clear experimental method to isolate the two components. This division is non-trivial since energy consumed in plastic dissipative processes depends on the geometry, loading, and various stages of crack growth. In this work, we pursue two different aspects of this question. First we would like to evaluate the contribution of plastic work towards total work, and then proceed to examine the various parameters that affect the quantity of plastic work.

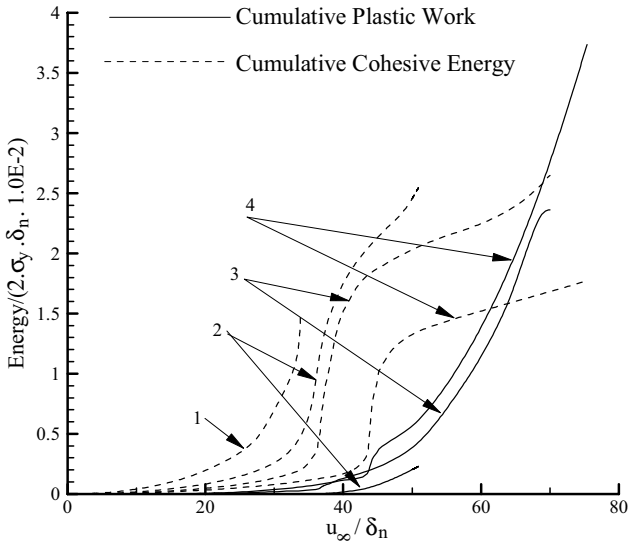

Figure 11 : Variation of cohesive energy and plastic energy for various $\sigma_{\max}/\sigma_y$ ratios. (1) $\sigma_{\max}/\sigma_y = 1.0$, (2) $\sigma_{\max}/\sigma_y = 1.5$, (3) $\sigma_{\max}/\sigma_y = 2.0$, (4) $\sigma_{\max}/\sigma_y = 2.5$.

Figure 11 shows variations of cohesive and plastic energy as the crack grows. We examine the effect of plasticity on the distribution of energy, and obtain different levels of plasticity by varying the ratio of $\sigma_{\max}/\sigma_y$. When a value of $\sigma_{\max}/\sigma_y = 1$ is used, the body experiences only elastic behavior while increasing this ratio to 1.5, 2.0 and 2.5 induces increasing levels of plasticity. By increasing the value of $\sigma_{\max}$ in the cohesive zone we are permitting a higher stress level within the bounding medium. Thus when $\sigma_{\max}/\sigma_y = 1$,it represents the elastic case where dissipation occurs only as cohesive energy. As the ratio is increased, increasing levels of plastic energy is dissipated. While plastic energy is considerably lower than cohesive energy in most of the cases, when $\sigma_{\max}/\sigma_y = 2.5$ (large scale plasticity), this is not true. In this case, significant plastic work is observed in latter stages of crack growth which will be quantified later.

Variation of Plastic work and cohesive work

Figure 12 shows the relationship between cumulative plastic energy and cohesive energy at various stages of crack growth for different values of $\sigma_{\max}/\sigma_y$. For the value of $\sigma_{\max}/\sigma_y = 1.5$ which represents very small scale plasticity, the plastic energy represents about 15% of the overall energy dissipated. In other words, the error in-

curred when plastic work is not accounted for in the dissipative processes is of the order of 15% when small scale plasticity is observed. In this case, plasticity occurs in the initial stage of crack growth, i.e., crack initiation rather than steady state growth. This implies that the deviation of 15% occurs during crack initiation leading to the fact that the rate of plastic energy dissipation will be much more significant in those stages.

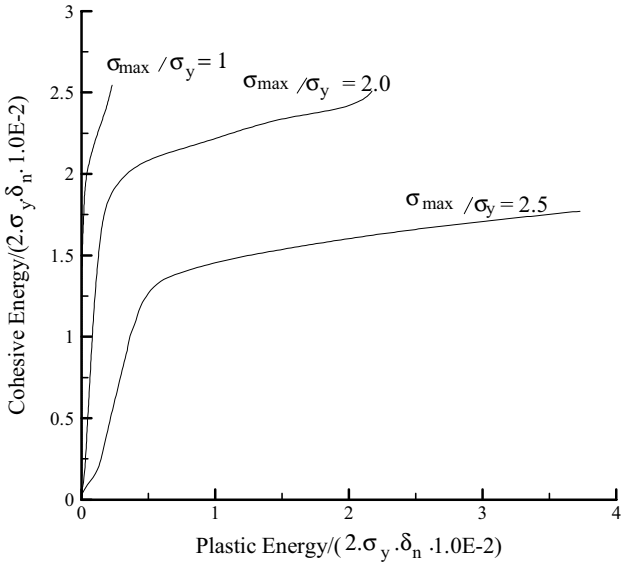

Figure 12 : Variation of plastic work with cohesive energy for different σ_{max}/σ_y ratio.

The figure 12 shows increasing levels of plastic work as a part of total dissipation when the values of $\sigma_{max}/\sigma_y \geq 2$. In these cases the amount of plastic work is significantly higher and is almost 100 % to 200% as that of cohesive energy. Obviously great care needs to be exercised in isolating plastic work from cohesive work in these cases. It is interesting to note that the input cohesive energy is of the order 8000 J/m^2 and is based on global fracture parameter K_{IC} or J_{IC}.

From the results shown in figure 11 and 12 it can be inferred that for crack growth to occur in a large scale plasticity case, a dissipative energy of much more than 8000 J/m^2 is necessary. Part of this energy will be used for plastic work and the rest in the fracture process as cohesive work. Whether the test results that formed the basis for the estimation of 8000 J/m^2 involved only fracture process or part fracture and part plasticity is not known. If we assume that during the test, no plasticity (or significantly low levels) occurred as in the case of very small scale yielding, then it is reasonable to assume that this 8000 J/m^2 represents only fracture work and not plastic work. Based on that assumption, it is possible to assign all the 8000 J/m^2 as the cohesive work. However, if the original test involved significant plastic work as the material is highly ductile then this value will represent both plastic and fracture work. A detailed study on spatial distribution of dissipative energies near the crack tip region are discussed in Shet and Chandra (2002).

Variation of Normal Traction along the interface

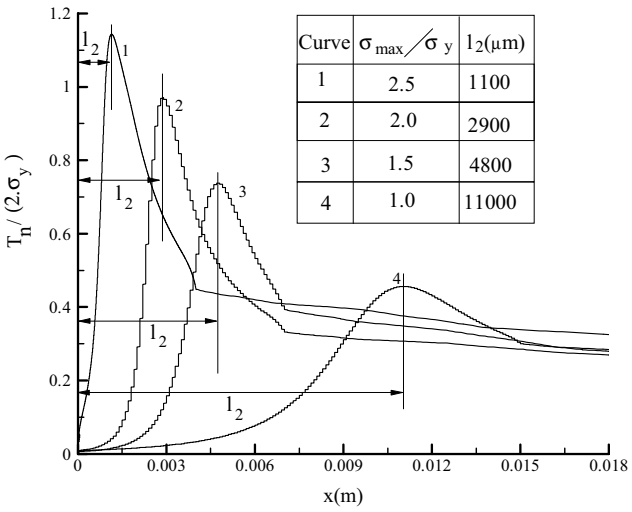

Figure 13 : Variation of the normal traction along the line of crack propagation for various σ_{max}/σ_y ratios. l_2 is the length of active cohesive wake.

Figure 13 shows the distribution of normal traction along the length of the interface. The length of active wake l_2 along which cohesive energy is dissipated are shown for various σ_{max}/σ_y ratios. The active wake length l_2 is longer when σ_{max}/σ_y ratio is small and it decreases with increased σ_{max}/σ_y ratios. In all the cases the input energy ϕ_n is same, and hence the post peak dissipation energy is also same. Because of this, for higher σ_{max}/σ_y ratios, the induced traction is higher, and hence δ_{sep} is smaller. This would make the active wake length smaller in case of higher σ_{max}/σ_y ratios when compared with that with lower σ_{max}/σ_y ratios.

6 Summary

Cohesive zone approach provides an alternative method of modeling fracture process (initiation, propagation and eventual failure) in continuous media. This approach is based on sound physics and micromechanics, and has the added advantage of easy implementation in numerical methods. We present a number of fundamental issues that need careful attention for successful application of CZM to model fracture. In this paper the issue of the origin of CZM in relation to the underlying micromechanisms is examined. Next the principle of the balance of energy in fracture is invoked to show that the area under cohesive response represents the sum total of all inelastic energy that flows into the crack tip. Additionally the paper addresses some of the key issues in obtaining cohesive zone parameters, (e.g. cohesive energy) in terms of measurable quantities. Some of the salient observations in this work are:

- In case of elastic material the entire fracture energy given by the J_{IC} of the material, is dissipated in the fracture process zone by the cohesive elements, as cohesive energy.

- In case of small scale yielding material, a small amount of plastic dissipation (of the order 15%) is incurred, mostly at the crack initiation stage. During the crack growth stage, because of reduced stress field, plastic dissipation is negligible in the forward region. The error accrued by neglecting plasticity with respect to dissipated energy is of the order 15% in this case. On the other hand in the case of large scale yielding, there is considerable plastic dissipation together with cohesive energy; neglecting plasticity here may lead to erroneous results.

- Plastic work depends on the shape of the crack tip in addition to $\sigma_{\max}/\sigma_y$. Before steady state conditions are established, the sharpness of the crack tip reduces from very sharp to blunt crack; the level of bluntness is dictated by the shape of the $T-\delta$ curve (l_1/l_2 ratio).

References

ABAQUS (1998): Manual, version 5.8, Hibbit, Karlsson & Sorensen, Inc, USA.

Allen, DH; Searcy, CR. (2001): A micromechanically-based model for predicting dynamic damage evolution in ductile polymers, Mech Mater. 33 (3), 177-184.

Barenblatt, G. I. (1959): The formation of equilibrium cracks during brittle fracture. General ideas and hypothesis. Axially-symmetric cracks, *PMM*, Vol.23, pp.434-444.

Barenblatt, G. I. (1962): Mathematical Theory of Equilibrium Cracks. *Advances in Applied Mechanics*, Academic Press, New York 7, pp.55-125.

Camacho, G. T.; Ortiz, M. (1996): Computational modeling of impact damage in brittle materials, *Int. J. Solids Structures*, Vol.33, pp.2899-2938.

Chandra, N.; Li, H.; Shet, C.; Ghonem, H. (2002): Some Issues in the Application of Cohesive Zone Models for Metal-Ceramic Interfaces, *Int. J. Solids Structures*, 39, pp.2827-2855.

Dugdale, D. S. (1960): Yielding of steel sheets containing slits, *J. Mech. Phys. Solids*, Vol. 8,100-104.

Eisenmenger, W. (2001): The mechanisms of stone fragmentation in ESWL, *Ultrasound Med. Biol.* 27 (5), pp. 683-693.

Geubelle, P. H.; Baylor, J. (1998): The impact-induced delamination of laminated composites: a 2D simulation, *Composites*, Vol.29B, p.589.

Hutchinson, J. W.; Evans, A. G. (2000): Mechanics of materials: Top-down approaches to fracture, *Acta mater.*, Vol.48, pp.125-135.

Li, H.; Chandra, N. (2003): Analysis of crack growth and crack-tip plasticity in ductile materials using cohesive zone models, *Int. J of Plasticity* 19 (6) pp.849-882.

Li, W.; Siegmund, T. (2004): Numerical Study of Indentation Delamination of Strongly Bonded Films by Use of a Cohesive Zone Model, *CMES: Computer Modeling in Engineering & Sciences*, Volume 5, No. 1, pp. 81-90.

Maiti, S.; Geubelle, P. H. (2004): Mesoscale Modeling of Dynamic Fracture of Ceramic Materials, *CMES: Computer Modeling in Engineering & Sciences*, Volume 5, No. 2, pp. 91-101.

Mukherjee, S. (1997): Effect of interfaces on the mechanical behavior of metal matrix composites: computational and experimental study. Dissertation of Ph. D, Florida State University.

Mukherjee, S.; Ananth, C. R.; Chandra, N. (1998): Effect of interface chemistry on the fracture properties

of titanium matrix composites. *Composites* Part A. 29A, 1213-1219.

Needleman, A. (1987): A continuum model for void nucleation by inclusion debonding, *J.Appl. Mech.*, Vol.54, pp.525-531.

Needleman, A. (1990a): An analysis of tensile decohesion along an interface, *J. Mech. Phys. Solids*, Vol.38, pp.289-324.

Needleman, A. (1990b): An analysis of decohesion along am imperfect interface, *Int. J of Fracture*, Vol.42, pp.21-40.

Rice, J. R. (1968): A path independent integral and approximate analysis of strain concentration by notches and cracks, *J. Appl. Mech.*, Vol.35, pp.379-386.

Rice, J. R.; Jian-sheng Wang (1989): Embrittlement of Interfaces by Solute Segregation, *Mater. Sci. Eng.* Vol.A 107, pp.23-40.

Ritchie, R. O. (1999): Mechanisms of fatigue-crack propagation in ductile and brittle solids, *Int. J. Fracture* 100, 55-83.

Shet, C.; Chandra, N. (2002): Analysis of energy balance when using cohesive zone models to simulate fracture processes, *Journal of Engineering Materials & Technology*, 124, pp.440-450

Tvergaard, V.; Hutchinson, J. W. (1992): The relation between crack growth resistance and fracture process parameters in elastic-plastic solids, *J. Mech. Phys. Solids*, Vol.40, pp.1377-1397.

Tvergaard, V. (1990): Effect of fibre debonding in a whisker-reinforced metal, *Mater. Sci. Eng.* Vol.A 125, pp.203-213.

Xu, X. P.; Needleman, A. (1993): Void nucleation by inclusion debonding in a crystal matrix, *Modelling Simul. Mater. Sci. Eng.*, Vol.1, pp.111-132.

Xu, X. P.; Needleman, A. (1994): Numerical simulation of fast crack growth in brittle solids, *J. Mech. Phys. Solids*, Vol.42, pp.1397-1434.

Yang, B.; Mall, S.; Ravi-Chandar, K. (2001): A cohesive zone model for fatigue crack growth in quasibrittle materials, *Int J Solids Struct* 38, pp. 3927-3944.

Zhang, P.; Klein, P.; Huang, Y.; Gao, H.; Wu, P. D. (2002): Numerical Simulation of Cohesive Fracture by the Virtual-Internal-Bond Model, *CMES: Computer Modeling in Engineering & Sciences*, Vol. 3, No. 2, pp. 263-278